14. G. I. Kanel' and V. V. Shcherban', "Plastic deformation and spalling in armco iron in shock waves," Fiz. Goreniya Vzryva, No. 4 (1980).
15. C. S. Speight, P. F. Taylor, and A. A. Wallace, "Observations of spallation and attenuation effects in aluminium and beryllium from free-surface velocity measurements," in: Metallurgical Effects at High Strain Rates, Plenum Press, New York–London (1973).

INVESTIGATION OF SPALLING FRACTURE UNDER SHOCK DEFORMATION. MODEL OF A DAMAGED MEDIUM

N. Kh. Akhmadeev

UDC 539.42:620.172.254

In connection with the diverse applications of the action of shocks in engineering and science, the question of the strength of the materials being tested under intensive dynamic action conditions is important. At this time the domain of static and quasistatic rupture under tension has been studied sufficiently well. The kinetic (thermofluctuation) theory of the strength of solids (yielding a dependence of the specimen longevity on the magnitude of the tensile stresses σ and on the temperature T), which is valid for fractures occurring in times from 10^{7}-10^{-3} sec [1] has received great acclaim. For fractures with a $\sim 10^{-6}$ sec time scale there is just a system of test facts that is still inadequate for the complete comprehension of processes occurring under dynamic fracture.

1. Dynamic Spalling Fracture

The spalling fracture of plates, finite thickness targets first subjected to shock loading occurring in very brief times ($\sim 10^{-6}$-10^{-7} sec) during head-on interaction of rarefaction waves moving from the plate free surfaces is considered. In collisions of rarefaction waves with intensity 13 GPa and higher, spall in iron and steel specimens is characterized by the formation of very smooth (specular) fracture surfaces [2] with high purity of the spall surfaces, and is the result of the rarefaction wave collisions in which the reverse $\varepsilon \rightarrow \alpha$ phase transformations are realized. As the level of the rupturing stresses is lowered, the purity of the spall surfaces becomes less and under the action of sufficiently high (4-5 GPa) tensile stresses the domains close to the spall surface are characterized by the presence of a large number of microdamage. This is indicated by available test data from a number of experimental papers on the collision of plates [3-6] in which it is made clear for the materials being tested (metals, polymers) that the intensive formation of microdamage (in the form of flat cracks or round pores) occurs in the zone of action of a tensile impulse, resulting in total fracture (rupture) as they accumulate to a certain critical level, in a section of the plate standing off from the external free surface at a distance approximately equal to the length of the impactor. Microdamages are formed in the rupture zone because of the destruction of the solidity in submicroscopic inhomogeneities (solid phases, particles of insoluble impurities, etc.) under the action of the tensile stresses as well as because of the exposure of already existent submicrocavities (gas bubbles, shrinkage cavities, blisters, etc.). At this time there are no direct methods that permit measurement of the stresses or strains (or other parameters) in the fracture domain, and the spall fracture process is determined by the experimentally determined velocity W(t) of the free target surface, by the thickness of the spalling layer δ^* and the structure of the zones close to the spall surface [3-5], hence, mathematical models must be relied upon to analyze the fracture process.

In investigating spall fractures caused by the action of tensile stresses on the order of 6-8 GPa and higher, and characterized by a quite short fracture delay time after the appearance of the tensile stresses, diagramming the instantaneous spall [7] is completely applicable when a mainline crack is formed immediately upon the attainment of a certain critical (rupture) stress σ^*, which divides the specimen into parts at the site where the stress σ first reaches the value σ^*. Attempts to utilize limit criteria based on the critical fracturing stresses σ^* and their various modifications (for example, taking account of the rate

Ufa. Translated from Zhurnal Prikladnoi Mekhaniki i Tekhnicheskoi Fiziki, No. 4, pp. 158-167, July-August, 1983. Original article submitted June 8, 1982.

 0021-8944/83/2404-0592$07.50

of stress growth in the section being fractured, etc.) to describe spall in waves of lower intensity did not result in satisfactory results since the formation of microdamage resulting in a delay in fracture and substantially changing the flow pattern in tensile waves with 4-5 GPa stresses and below becomes the predominant factor in fracture. As the microdamage grows, a diminution in the mean stress first occurs in the macroparticle of the damaged medium [8], and the possibility of introducing a certain maximal σ^*, although even provisionally, raises doubts. Moreover, under similar conditions, specimen fracture occurs with a lag, and is developed in a certain time after which tensile stresses occur that are sufficient for the formation of local damage, hence, the appearance and accumulation of microdamage in the material, that are responsible for the spalling fracture mechanism, and the possibility of their partial or total closure under reverse compression must be taken into account. The need to introduce measures of the damage or a damageability function in the description of fracture in solids was understood long ago by researchers (see [9], for instance). Up to now a number of models has been developed in which a continuous measure of damage, usually identified with the volume content of vacancies, is introduced to describe spalling fracture. A spalling fracture model is developed in [5] for the action of a tensile pulse with the generation of a definite number of initial microcracks or micropores of fixed dimensions, and then their growth by the exposure of the microdamage being formed also taken into account. Complete separation of part of the specimen occurs because of the merger of the microvacancies into a single microcrack. Results of a detailed investigation of fractured specimens are used in [5], in which the microfractures are classified by shape, and size, and their volume distribution as a function of size is determined, and in the case of microcrack formation, as a function of their orientation also. The fracture being characterized by the formation of microcracks (having the shape of a flat disk) is called brittle, this kind of fracture was observed in armco iron specimens. When almost spherical microvacancies are formed in the rupture zone (as is characteristic for aluminum specimens), the fracture is defined as viscous. It should be noted that the computational models proposed in [5] are overloaded with kinetic constants used to describe the kinetics of microdefect generation and the rate of their opening. An example of using such a model to describe the fracture in copper specimens is presented in [10]. A somewhat simpler spalling fracture scheme as the result of cumulative damage dependent on the applied stress and on the already existing fracture, is used in [11]. The model of the fracture viscoplastic media with cumulative damage and taking account of their influence in shear stresses is constructed in [12].

A model of a damaged medium is proposed in this paper, which takes account of the process of microdamage formation under the effect of tensile stresses that are capable of developing with the lapse of time into macrofracture in the form of spall cracks dividing the loaded specimens into parts. In order not to complicate, and without any sufficiently complex model of a flow with fractures, an elastic—plastic model is considered in which the main attention is turned to the process of microdamage, the determination and investigation of the kinetics of their growth in tension waves. Not very weak waves (with a 4-5 GPa stress level) are considered here, and if necessary the viscoplastic properties of deformable media can be taken into account in waves of lower level on the basis of dislocation representations [13].

2. Equations of the Model

Let us consider the motion of a damagable condensed medium in which there are microcavities. Such a medium can be represented as a mixture of two phases [14], each of which occupies a certain part of the total mixture volume V and on whose interphasal surfaces the macroscopic characteristics of the medium (the density, say) undergo a discontinuity. Let the first phase be the undamaged part of the carrying medium (we henceforth call it the matrix) that occupies the volume V_m and is characterized by the true density ρ^0. The second phase is the microcavities occuping the volume V_ξ with the true density of the cavity (gas) material $\rho^0{}_\xi$, where the evident inequality $\rho^0{}_\xi \ll \rho^0$ is satisfied. Shown as an illustration in Fig. 1 is a cubic macrovolume V of a damageable medium with linear macroscopic dimensions l, in which microvolumes of the matrix of the carrying medium V_m' and the cavities V_ξ' with the characteristic dimensions $\lambda \ll l$ are isolated. It is clear that summation of the mentioned microvolumes V_m' and V_ξ' over the whole macrovolume of the mixture ($V \gg V_m'$, V_ξ') will yield the total volumes of the mixture phases, respectively

$$V_m = \sum_V V_m' \quad \text{and} \quad V_\xi = \sum_V V_\xi',$$

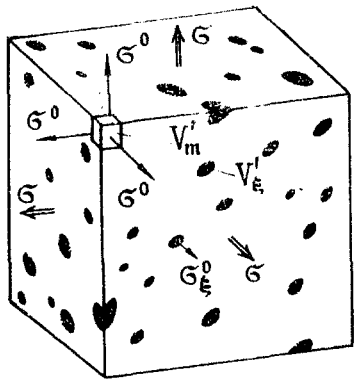

Fig. 1

which indeed comprise the initial mixture volume V, i.e., $V = V_m + V_\xi$. Let us define the specific volume content of the microdamage ξ as the ratio V_ξ/V, then the relation

$$\rho = \rho^0(1-\xi) + \rho^0_\xi \xi \approx \rho^0(1-\xi). \tag{2.1}$$

holds for the mean density ρ of the damageable medium.

Let us write down the mass, momentum, and energy conservation laws in the one-dimensional plane case for the average quantities of the damageable medium

$$\frac{1}{\rho}\frac{d\rho}{dt} = -\frac{\rho}{\rho_0}\frac{\partial u}{\partial r}, \quad \rho_0 \frac{du}{dt} = -\frac{\partial \sigma}{\partial r}, \quad \rho_0 \frac{de}{dt} = \sigma \frac{\partial u}{\partial r}. \tag{2.2}$$

which are valid to a certain critical value of the bulk content of the microdamage ξ^*. Upon reaching ξ^* it is impossible to describe the damageable medium by the methods of continuum mechanics. It is natural to relate this critical value of ξ^* to the formation of macrodamage, when fracture of the skeleton of the matrix of the carrying medium occurs in a certain flow domain and the damageable medium in this domain is transformed into a set of separate microparticles of the condensed phase (powders). The fracture zone can be one or several through macrocracks separating the specimen into individual macroblocks, or macrocavities within the specimen that contain microparticles of the initial phase.

The following notation is used in (2.2): u is the mass flow rate of mixture particles, e and σ are the specific internal energy and the average stress tensor of the damageable medium (see Fig. 1), which are representable in terms of the appropriate quantities e^0 and σ^0 of the undamaged matrix material (called the true quantities) in the form

$$e = e^0 + e^0_\xi + e^s_\xi, \quad \sigma = \sigma^0(1 - F(\xi)) + \sigma^0_\xi \Phi(\xi), \tag{2.3}$$

where e^0_ξ and σ^0_ξ are the specific internal energy and stress of the microcavity material, and $e^s{}_\xi$ is the energy associated with the formation of microcavity surfaces of volume ξ. The material of the microdamage phase is the gas or mixture of gases dissolved in the matrix (accompanying the technological process of fabricating the initial condensed medium, possibly partially rarefied), for whose parameters $e^0_\xi = e^0$ and $\sigma^0_\xi = \sigma^0$ are valid relative to the carrying condensed phase parameters as for the densities ρ^0_ξ and ρ^0. Examples can be presented when it is impossible to neglect the quantities ρ^0_ξ, e^0_ξ and σ^0_ξ of the gas phase being formed in the initial solid medium. In particular, upon detonation of solid explosives the density, pressure, and internal energy of the gaseous detonation products being formed during the chemical reactions are commensurate, in order of magnitude, with the corresponding solid phase quantities, and they should be taken into account in full measure [15]. In (2.3) the $F(\xi)$ and $\Phi(\xi)$ are functions of the microdamage shapes. In the simplest case $F(\xi) = \Phi(\xi) = \xi$. The necessity to take account of the microdamage shape in the model is because the volume of a unit microcrack in the shape of a flat disc (even when the disc radius agrees with the pore radius) is less than the volume of a unit spherical micropore. Hence, in the formation of plane microcracks (ξ_c) with spherical micropores (ξ_p) of identical specific bulk content $\xi_c = \xi_p$, the quantity of microcracks N_c and their total surface S_c (which is interphasal in the damageable medium) is greater than the corresponding quantities N_p and S_p for the micropores. Consequently, the average stress σ being realized in an arbitrarily separated macroarea S in the damageable medium depends on the shape of the microdamage, and for the microcracks on the orientation also. The internal energy and stress in the undamaged microvolumes

of the carrying medium are determined by the relationships $e^\circ = e^\circ(\rho^\circ, T)$ and $\sigma^\circ = -p^\circ(\rho^\circ, T) + \tau^\circ$, in which the Mie–Grüneisen equation of state [16] can be used to describe $e^\circ(\rho^\circ, T)$ and $p^\circ(\rho^\circ, T)$. The Hooke's law

$$\frac{d\tau^0}{dt} = -\frac{4}{3}\frac{\mu}{\rho^0}\frac{\partial\rho^0}{\partial t} \quad \text{for} \quad \tau^0 < \tau_s \tag{2.4}$$

is assumed valid for the stress deviator in the elastic domain. In the plastic flow domain, when $\tau^\circ \geqslant \tau_s$, the deviator τ° is conserved at the yield point in conformity with the Mises flow condition. In (2.4) the μ and τ_s are the effective shear modulus and the yield point in the macroparticle of the damageable medium, taking into account that these characteristics should be diminished as compared with μ° and τ_s° of the undamaged material in a material weakened by microdamage. We assume that this change, as for σ also, depends on the shape of the microdamage being formed: $\mu = \mu^\circ(1 - F(\xi))$, $\tau_s = \tau_s^\circ(1 - F(\xi))$. Taking account of (2.1), and the mass conservation law (2.2), the relationship (2.4) can be transformed into

$$\frac{d\tau^0}{dt} = \frac{4}{3}\mu\left[\frac{\rho}{\rho_0}\frac{\partial u}{\partial r} - \frac{1}{1-\xi}\frac{d\xi}{dt}\right], \tag{2.5}$$

which shows that the deformation due to microvoid growth (see the second term in (2.5)) must be taken into account in determining the deviator τ° in the total deformation of the damageable medium (see the first term in (2.5)).

3. Damage Kinetics

It is detected [3] in performance of spalling rupture experiments that the degree of medium damage under dynamic tension depends on the intensity of the tension wave σ° and the time of action of the applied stress. There are experimental data that indicate that the formation and growth of damage depend on the structural parameters η_i, for instance, on the species of material being tested [5], and the mechanical characteristics of the specimens (grain size, mechanical impurities, orientation of the preliminary mechanical treatment, etc.). It was clarified in [4] that other conditions being equal an identical degree of damage (total spall, say) can be achieved in a wave of somewhat lower intensity if the direction of action of the tensile forces were perpendicular to the technological rolling direction. It is shown in [17] that the initial material graininess (copper specimens were tested) also influences the fracture process, and other conditions being equal a diminution in the grain size from 250-350 to 60-70 μm would result in a lower degree of specimen damage (from total spall to initial microdamage, respectively). There are data about the influence of preliminary heat-treatment (annealing) and the initial heating temperature T_0 of the specimens [18] on the spalling process. Moreover, the already existent microdamage ξ should also evidently influence the growth of damage. Therefore, it can be considered that the kinetics equation has the form

$$\dot{\xi} = f(\sigma^0, \xi, T_0, \eta_i), \tag{3.1}$$

and it can be assumed that the submicrodefects existent in real materials (stress concentrators and submicrovoid seeds) are distributed uniformly over the volume and are sufficiently many in number in each elementary microvolume V′ of the material being tested; otherwise sections of the specimens could be isolated that would possess the theoretical rupture strength [19]. Keeping the data of [1] in mind, we note that the kinetics (3.1) can be separated into two successive stages, i.e., be represented as

$$\dot{\xi} = \psi(\sigma^0, \xi_0, T_0, \eta_i) + f(\sigma^0, \xi).$$

The first stage is the preliminary kinetic process corresponding to the formation of submicrocavities of the size $\zeta (\zeta \ll \lambda)$. Under the action of tensile stresses σ° on the solid submicrodefects (particles of undissolved impurities, solid phases, etc.) a break in the continuity of the carrying medium occurs because of the stress concentration, and then they open together with the seed submicrocavities already existent in the initial medium (the gas bubbles and blisters) of the bulk content ξ_0. The second stage is the growth of microdamage from submicrophases of the size ζ to certain (limiting) stable microsizes λ. We note the following here: The formation of macrodamage with characteristic macroscopic dimensions l should not be understood as the growth of a unit microcavity of dimension λ (or volume V_ξ') to the macrodimension l (or to the volume V_ξ, commensurate with V). Macrofracture can yield only a collective of microdamage, each of which has its limiting linear scale dimension λ, and will reach the critical level of the bulk content $\xi^* = V_\xi^*/V$ in a set. The achievement of

the critical level ξ^* results in rather strong attenuation of the strength of the matrix of the carrying medium, which is fractured completely in the domain of its skeleton under consideration.

At this time there are practically no test data about the fracture parameters at the sub- and microlevels for the determination of the function ψ. Existing experimental material yields mainly macroscopic fracture parameters, the length and flight velocity of the spalling layer, and only in very few papers, for instance, in [3-5], are there information about the limiting size λ of the microdamage being formed. Hence, we shall consider that when the tensile stress σ^0 exceeds a certain level σ_L in the matrix of the carrying medium, then the formation of microdamage of the size λ will occur according to the following kinetics:

$$\dot{\xi} = f(\sigma^0 - \sigma_L,\ \xi) \quad \text{for} \quad \xi < \xi^* \text{and} \sigma^0 > \sigma_L\,, \tag{3.2}$$

where the function f can be determined by modeling the conditions of real experiments.

It is shown in [5] and then in [20] that separation of the specimen occurs when ξ achieves a magnitude on the order of 7-10% (i.e., ξ^*) in a certain section. For $\xi = 0$ the stress σ in a macroparticle of damageable medium will agree with the true stress σ^0, while $F(\xi) = 0$. As ξ grows, the average stress σ diminishes and for $\xi = \xi^*$ the quantity is $F(\xi) = 1$, while simultaneously the stress is $\sigma = 0$, which will correspond to total fracture of the macroparticles, although the true stress σ^0 can indeed be different from zero at this instant in its individual microparticles. As the damage ξ grows the threshold level of the fracturing stresses σ_L should diminish (compared with the level σ_L^0 needed to form damage in a monolithic specimen), for which we take $\sigma_L = \sigma_L^0(1 - F(\xi))$ analogously to (2.3), by assuming that additional damage can be caused by already lower tensile stresses σ^0 in the specimen macroparticle being tested, which is weakened by microdamage.

It follows from an analysis of experiments on spalling fracture by the impact of plates with velocity v_0, when a sufficient duration of the wave impulse is realized, that for fixed materials and an impactor and target length of $l_1 - l_2$ it is possible to introduce: the threshold velocity of the plate impact v_s corresponding to the beginning of the intensive seeding and opening of the submicrocavities (for whose determination experiments are required with a study of the structure of the specimens being loaded at the sub- and microlevels); the threshold velocity V_m corresponding to the beginning of the formation of microdamage (denoted by v_1 in [3]) and dependent on the selection of that level of submicrocavity volume which will be taken as the passage to microdamage (it is correctly noted in [3] that the velocity v_1 determined experimentally corresponds to damage which is not initial), the threshold impact velocity v_f resulting to macrodamage, spall cracks separating the specimens into parts because of cumulative micro- to macrodamage (denoted by v_2 in [3]), and finally, the threshold velocity v_d denoting the passage to spall macrofracture with preliminary formation of microdamage (i.e., smooth or rough). The introduction of threshold impact velocities permits separation into experiments with $v_0 < v_s$, $v_s \leqslant v_0 < v_m$, $v_m \leqslant v_0 < v_f$, $v_f \leqslant v_0 < v_d$, $v_0 \geqslant v_d$, which corresponds to no fracture at the target, the formation and opening of submicrodamage with characteristic size ζ, the formation of macrodamage of size λ comparable to the macroscopic dimensions of the specimens being tested ($\zeta \ll \lambda \ll l$) and being characterized by the delay of fracture determined by the kinetics (3.1), and the formation of through macrocracks in a specimen without the delay in fracture. Such a classification of the impact velocity v_0 affords the possibility, say, of explaining the existing difference in the interpretation of experiment data in [6] and [18] on the influence of the initial heating of the specimens T_0. Specimens of annealed aluminum ($l_2 = 5$-40 mm) were loaded by a hollow aluminum vessel ($l_1 \approx 2$ mm) at a velocity v_0 from 300-1200 m/sec at the initial temperature 20 and 320°C in [6]. In all the experiments, complete spall and autonomous motion of the spalling layer δ^* were observed on the interferograms of the free surface velocity W(t). The processing of the experimental measurements performed in [6] showed that the selected values of the initial temperature T_0 do not influence the spall, and in particular, the dependence of the specimen longevity on the maximal rupturing stress, in which connection a deduction is made in [6] about the athermy of the spalling fracture process. In [18] a dependence of the critical impact velocity v_* (for which damage formation is still not observed visually) on the initial temperature T_0 is obtained for a number of metals. A 5% increase in v_* resulted in partial fracture in the form of local macrocracks, and a subsequent increase in the impact velocity resulted in the separation of the spalling layer in the central part of the specimen, being accompanied by the growth of the surface of separation because of the opening of the mainline macrocracks along the edges. In a first approximation it can be considered for

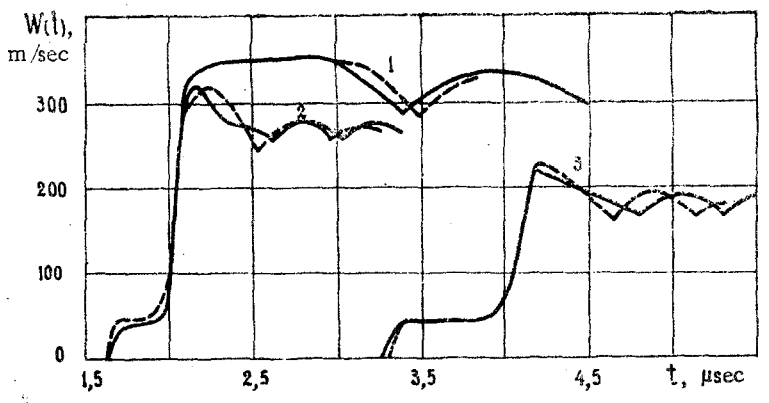

Fig. 2

an upper bound that $v_m \approx v_*$, while $v_f \approx (1-0.05)v_*$. In [18], the velocity $v_* \approx v_m = 253$ m/sec is determined for a 20-mm-long plate of unannealed aluminum AD-1 loaded at $T_0 \approx 0°C$ by impact from a AMts alloy with $l_1 = 4$ mm, while $v_f \approx 265$ m/sec. Interpolation of experimental data for the temperature $T_{00} = 20°C$ (normal initial conditions) yields the velocity values $v_{m0} \approx 247$ m/sec, $v_{f0} \approx 260$ m/sec, and $v_m \approx 168$ m/sec and $v_f \approx 176$ m/sec, respectively, for $T_0 = 320°C$. It is also clarified in [18] that under conditions close to normal, preliminary annealing diminishes the velocity v_* by approximately 10%, while the dependence $v_*(T_0)$ for annealed material (copper) approaches the dependence $v_*(T_0)$ for unannealed material as T_0 increases, and agrees with it for $T_0 \geqslant 600°C$.

It follows from the data presented above that in all the tests [6] the condition $v_0 > v_f$ was satisfied, which is strengthened if the following is taken into account: Annealed specimens of aluminum (which yields a diminution in v_f for $T_0 \approx T_{00}$) were tested in [6], moreover, for $T_0 > T_{00}$ the velocity v_f diminishes as T_0 grows. It is clear that when the tension wave energy exceeds the energy needed for spall (i.e., for $v_0 > v_f$), it is difficult to expect noticeable influence of the temperature on the spall process for $20° \leqslant T_0 \leqslant 320°C$. The situation is different when the tension wave energy is close to the spall energy ($v_0 \approx v_f$). Under these conditions the influence is shown in [18] of the temperature T_0 on the magnitude of the threshold velocities v_m and v_f and on the spall kinetics for $T_0 > T_{00}$ and $T_0 < T_{00}$.

4. Numerical Results

The model of a damaged medium was used for a numerical description of the spalling fracture of plates under experiment conditions [12]. An Armco-iron target was loaded by impact of an aluminum plate at a velocity of $v_0 \approx 600$ m/sec in [12]. The following three pairs of plates $l_1 - l_2$ (in mm) were tested: 5-10, 2-10, 2-20, for which the velocity profile of the external free target surface W(t) was recorded by a capacitive method. Several versions of the kinetic equation (3.3) were considered in the model computations, which showed that the following kinetics works well enough:

$$\dot{\xi} = \frac{\sigma^0 - \sigma_L}{\tau_K \sigma_L^0}(1+\xi) \quad \text{for} \quad \xi < \xi^* \text{ and } \sigma^0 > \sigma_L = \sigma_L^0(1 - F(\xi)),$$

which agreed satisfactorily with existing experimental and computational facts. The computational data for the experiments [12] are presented in Fig. 2 in the form of velocity profiles for the free target surface W(t) (curve 1 for the pair 5–10; curve 2 for the pair 2–10; and curve 3 for the pair 2–20) obtained for the following values of the kinetic constants $\tau_K = 0.07$ μsec; $\sigma_L^0 = 1.8$ GPa; $\xi^* = 0.075$; $F(\xi) = (\xi/\xi^*)^{1/2}$; $e^S{}_\xi = 0$. It is seen from Fig. 2 that the computed (solid lines) and experimental (dashed lines) data are in good enough qualitative agreement. The greater misalignment in curves 3 for a 20-mm-long target is possibly caused by the influence of side unloading. Analysis of the test conditions [12] showed that the impact velocity v_0 realizable is greater than the corresponding threshold velocity v_f for the pairs of plates $l_1 - l_2$ being tested. To describe the fracture in the broader range of loading, information is needed about the collision of the plates (we assume the 2—10 pair) at lower impact velocities close to v_f when partial damage ($v_0 < v_f$) and initial total spall ($v_0 \approx v_f$) would be realized. The total compression impulse formed in the target when testing the plates 5—10 is shown in Fig. 3b. The direction of motion of the

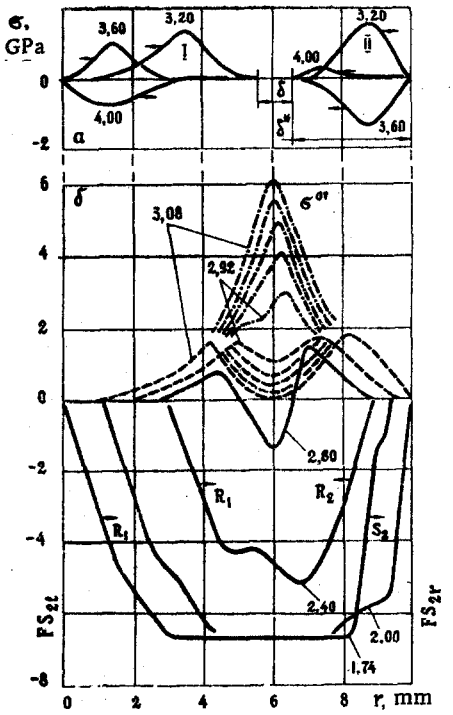

Fig. 3

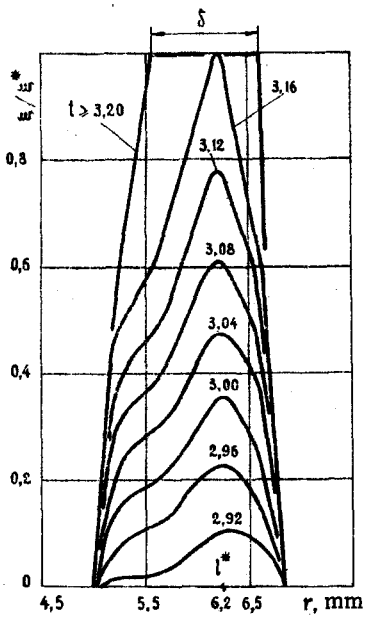

Fig. 4

compression S_2 and rarefaction fronts R_1 is shown by arrows in the diagrams of $\sigma(r)$. After emergence of the forward front of the compression pulse S_2 on the right free surface of the target FS_{2r} (see the $\sigma(r)$ diagram for $t = 2.00$ μsec), the formation of the unloading wave R_2 moving back from the surface FS_{2r} occurs. The location of the opposite rarefaction waves R_1 and R_2 is shown by the $\sigma(r)$ diagram at $t = 2.40$ μsec. The collision of the waves R_1 and R_2 results in the formation of a tensile pulse. The tensile stress diagrams $\sigma^{0'}$ presented in Fig. 3 in the form of dash—dot lines at the times $t = 2.92$, 2.96, 3.00, 3.04, 3.08 μsec were computed under the assumption that damage does not occur in the target for any tensile stress intensity. At the same times, but in the form of dashed lines, the diagrams σ obtained with the microdamage (microcracks) being formed being taken into account, are represented. Comparison of the results obtained (compare the dash—dot and dashed lines) shows the strong influence of the microdamage being formed on the whole flow pattern. The growth of the specific bulk content of the microdamage in the target at the same times t is shown in Fig. 4. It follows from the data in Fig. 4 that the damage zone is localized in the middle part of the target, while the most dangerous section is at the depth $l^* = 6.2$ mm. It is seen from the $\sigma(r)$ and $\xi(r)$ diagrams at $t = 2.92$ μsec that the formation of microdamage of even a very small quantity will result in considerable stress relaxation $\sigma(r, t)$. At the time $t = 3.16$ μsec fracture of the skeleton of the target matrix and formation of through macrocracks occur at the depth l^*. Shown in Fig. 3a are the domain of total target fracture δ (see Fig. 4, also) and the length of the separating layer δ^*. At the times $t = 3.20$, 3.60, 4.00 μsec the further evolution of the separating tension pulses I and II acting in the remaining (larger) part of the target and the layer being isolated δ^* is shown by $\sigma(r)$ diagrams here. According to the output of the tension pulse II on the external undamaged free surface FS_{2r}, its reflection occurs in the form of a compression pulse (see the $\sigma(r)$ diagrams at $t = 3.20$ and 3.60 μsec). For the return motion and reflection of the compression pulse from the internal free surface layer δ^*, which has a damaged (cracked) surface, noticeable attenuation in the newly formed tension wave is observed (see the $\sigma(r)$ diagrams at the times $t = 3.60$ and 4.00 μsec).

Now, let us examine a series of experiment tests [21] in which a steel St. 3 target of different lengths ($l_2 = 5$, 10, 20, 25, 30, and 40 mm) was loaded by a steel impactor ($l_1 = 1.06$ mm, $v_0 = 960$ m/sec). Test data taking account of the measurement errors for δ^* and w^* mentioned in [21] (the mean flight velocities of the spalling layer) are represented as rectangles in the coordinate plate (δ^*, w^*) in Fig. 5. Numerical results obtained, respectively, by using instantaneous spall [7] and a damaged medium model schemes, are shown by

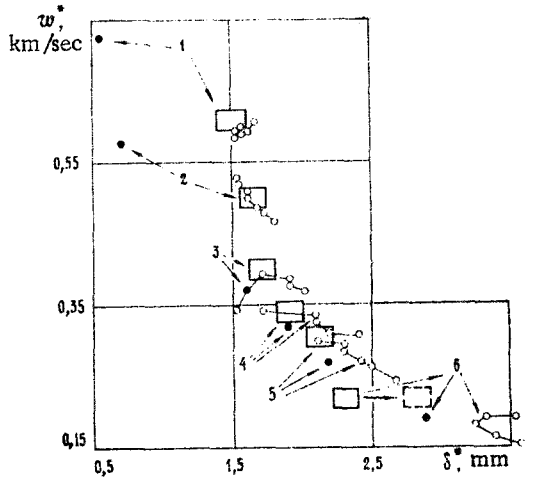

Fig. 5

the points I and II. The data presented in Fig. 5 confirm the deductions made in [7]. In particular, the instantaneous spall scheme (points I) describes tests 1 and 2 quite well, while there is a considerable discrepancy in the results obtained by using the damaged medium model (points II) for these tests. This is conceivable since spalls almost smooth are realized in tests 1 and 2. Conversely, good correspondence is observed for points II and tests 3-5, when spalling fracture is determined in longer targets as the intensity of the tension pulse being formed is reduced (because of shock damping in the bulk of the specimen) by the microdamage formation and accumulation. Analysis of the data represented affords a possibility to assume that the threshold impact velocity v_d is realized under the conditions considered for pairs of plates that are close to the pair tested in test 3 (l_1 =1.06 mm, l_2 =20 mm, v_d =960 m/sec). The existing mismatch for test 6 is caused by inaccuracies in restoring the length δ^* in the tests (see [7]), and the possible field of values of δ^* and w^* is marked by dashed lines in Fig. 5.

In conclusion, we note that energetic expenditures e_ξ^s that go into the formation of microdamage surfaces can be taken into account in the damaged medium model. For $e_\xi^s = e_\xi^* \xi / \xi^*$ in (2.3) numerical experiments are performed in which the quantity e_ξ^* was estimated preliminarily (e_ξ^* is the energy needed to form the fracture surface of the volume ξ^*), and then was variated in sufficiently broad limits. These computations showed that the influence of the quantity e_ξ^s on the spall fracture process is small is the proposed model, and the governing factor in the dynamic spalling fractures is the formation, growth, and accumulation of microdamage. The results represented in the paper show that the damageable medium model permits qualitative and quantitative description of existent experimental facts, conception and analysis of the fracture condition in the unloading waves, and classification of the spalling fracture of plates by the introduction of the threshold impact velocities v_s, v_m, v_f, and v_d. For further detailing of the model, experimental data are needed not only at the macrolevel (fixing the spall crack and the presence of damage) for different impact velocities but also at the microlevel, the determination of the threshold impact velocities corresponding to the beginning of the growth of sub- and microdamage, the quantitative estimation of microdamage, the study of damage zone structure, etc.

The author constantly used the attention and comments of R. I. Nigmatulin in the research and is deeply grateful to him.

LITERATURE CITED

1. V. R. Regel', A. I. Slutsker, and É. E. Tomashevskii, Kinetic Nature of the Strength of Solids [in Russian], Nauka, Moscow (1974).
2. A. G. Ivanov, S. A. Novikov, and Yu. I. Tarasov, "Spall phenomena in iron and steel caused by rarefaction shock interaction," Fiz. Tverd. Tela, 4, No. 1 (1962).
3. B. A. Tarasov, "On a quantitative description of spall damage," Zh. Prikl. Mekh. Tekh. Fiz., No. 6 (1973).
4. B. A. Tarasov, "Resistance to fracture of plates under impact loading," Probl. Prochn., No. 3 (1974).

5. L. Seaman, D. R. Curran, and D. A. Shockey, "Computational models for ductile and brittle fracture," J. Appl. Phys., 47, No. 11 (1976).
6. N. A. Zlatin, G. S. Pügachev, et al., "Time dependence of metal strength for microsecond band longevities," Fiz. Tverd. Tela, No. 9 (1975).
7. N. Kh. Akhmadeev and R. I. Nigmatulin, "Modeling of spall fracture under impact deformation, analysis of instantaneous spall schemes," Zh. Prikl. Mekh. Tekh. Fiz., No. 3 (1981).
8. M. Carroll and A. C. Holt, "Suggested modification of the p—α model for porous material," J. Appl. Phys., 43, No. 2 (1972).
9. Yu. N. Rabotnov, Creep of Structure Elements [in Russian], Nauka, Moscow (1966).
10. A. I. Glushko, "Investigation of spall as a micropore formation process," Izv. Akad. Nauk SSSR, Mekh. Tverd. Tela, No. 5 (1978).
11. L. Davison, A. L. Stevens, and M. E. Kipp, "Theory of spall damage accumulation in ductile metals," J. Mech. Phys. Solids, 25, No. 1 (1977).
12. G. I. Kanel' and V. V. Shcherban', "Plastic deformation and spall fracture of Armco iron in a shock," Fiz. Goreniya Vzryva, No. 4 (1980).
13. R. I. Nigmatulin, N. Kh. Akhmadeev, and N. N. Kholin, "Physicochemical processes in solids under explosive loading," in: Collection of Reports of the International Symposium Nonlinear Deformation Waves [in Russian], Pt. 2, Tallin (1977).
14. R. I. Nigmatulin, Principles of the Mechanics of Heterogeneous Media [in Russian], Nauka, Moscow (1978).
15. N. Kh. Akhmadeev, "Modeling of detonation waves in solid explosives," Fiz. Goreniya Vzryva, No. 1 (1981).
16. V. N. Zharkov and V. A. Kalinin, Equations of State of Solids at High Pressures and Temperatures [in Russian], Nauka, Moscow (1968).
17. O. A. Kleshchevnikov, V. I. Sofronov, et al., "Experimental confirmation of fracture criteria in tests with copper specimens," Zh. Tekh. Fiz., No. 8 (1977).
18. V. K. Golubev, S. A. Novikov, et al., "Influence of temperature on the critical conditions for spall fracture of metals," Zh. Prikl. Mekh. Tekh. Fiz., No. 4 (1980).
19. N. Kh. Akhmadeev and N. A. Akhmetova, "Kinetics of dynamic fracture in unloading waves," Abstracts of Reports. Fifth All-Union Congress on Theor. and Appl. Mechanics [in Russian], Nauka, Moscow (1981).
20. R. I. Nigmatulin, N. Kh. Akhmadeev, and N. A. Akhmetova, "Fracture of Armco-iron plates in unloading waves," in: Detonation. Physical Properties of Substances in Shocks [in Russian], Chernogolovka (1981).
21. A. P. Rybakov, "Fracture in steel for loadings by using the explosion of an explosive sheet charge and impact by a plate," Zh. Prikl. Mekh. Tekh. Fiz., No. 1 (1977).